The University of Arizona
Department of Planetary Sciences
Lunar and Planetary Laboratory

Galileo Net Flux Radiometer Report
1997

Martin G. Tomasko

NASA-Ames Award № NAG 2-906
UA FRS № 346170
FINAL

Galileo Net Flux Radiometer report—1997

On 7 December 1995, the Galileo probe entered Jupiter's atmosphere. The Net Flux Radiometer (NFR) on board the probe, measured upward and downward fluxes in the visible and infrared. At the University of Arizona, we have analyzed the data from the two visible-light channels, as well as the solar contributions to the thermal channels. The results are being prepared for submission to JGR in early September.

Overview of Net Flux Radiometer measurements

The NFR had five spectral channels: A (3-200 μm), C (3.5-5.8 μm), and D (14-200 μm) measured thermal fluxes, and the analyses of these was primarily done by University of Wisconsin personnel; channels B (0.3-3.5 μm) and E (0.6-3.5 μm) are sensitive to broad band solar and infrared solar radiation, respectively. The analysis of the latter two was primarily carried out at the UA. In addition to the spectral channels, a "blind" channel was included as a witness to non-radiative perturbations, which were significant. Data were obtained from about 0.4 bars to about 15 bars. Sromovsky *et al.* corrected the net flux observations by subtracting from each channel a non-radiative term proportional to the blind channel's observations ($NF_{corrected} = NF_{channel} - M_{channel} * (GAIN_{channel} / GAIN_{blind}) * NF_{blind}$; $M_B = 0.75 \pm 0.10$ and $M_E = 1.30 \pm 0.05$). A similar correction has been applied to the up fluxes ($M_B = 0.9 \pm 0.1$ and $M_E = 2.0 \pm 0.2$). In Figure 1, corrected up and net flux profiles are shown for low, nominal and high values of the correction factor.

The channel A and C measurements had some contribution from direct sunlight, necessitating close collaboration between UA and UW, including two visits by Mark Lemmon to UW in March and June 1997. In addition, the non-radiative contribution to the measurements is only partly understood, and is currently being investigated at the UW.

The measurements are made by chopping up and down at 2 Hz, and reporting the accumulated difference every six seconds (one integration cycle). In addition, the up flux is measured by chopping between down-looking and looking at an internal black body once each data cycle (20 integration cycles). The contribution of non-radiative effects to the up flux is not yet understood.

Investigation of the solar pulse

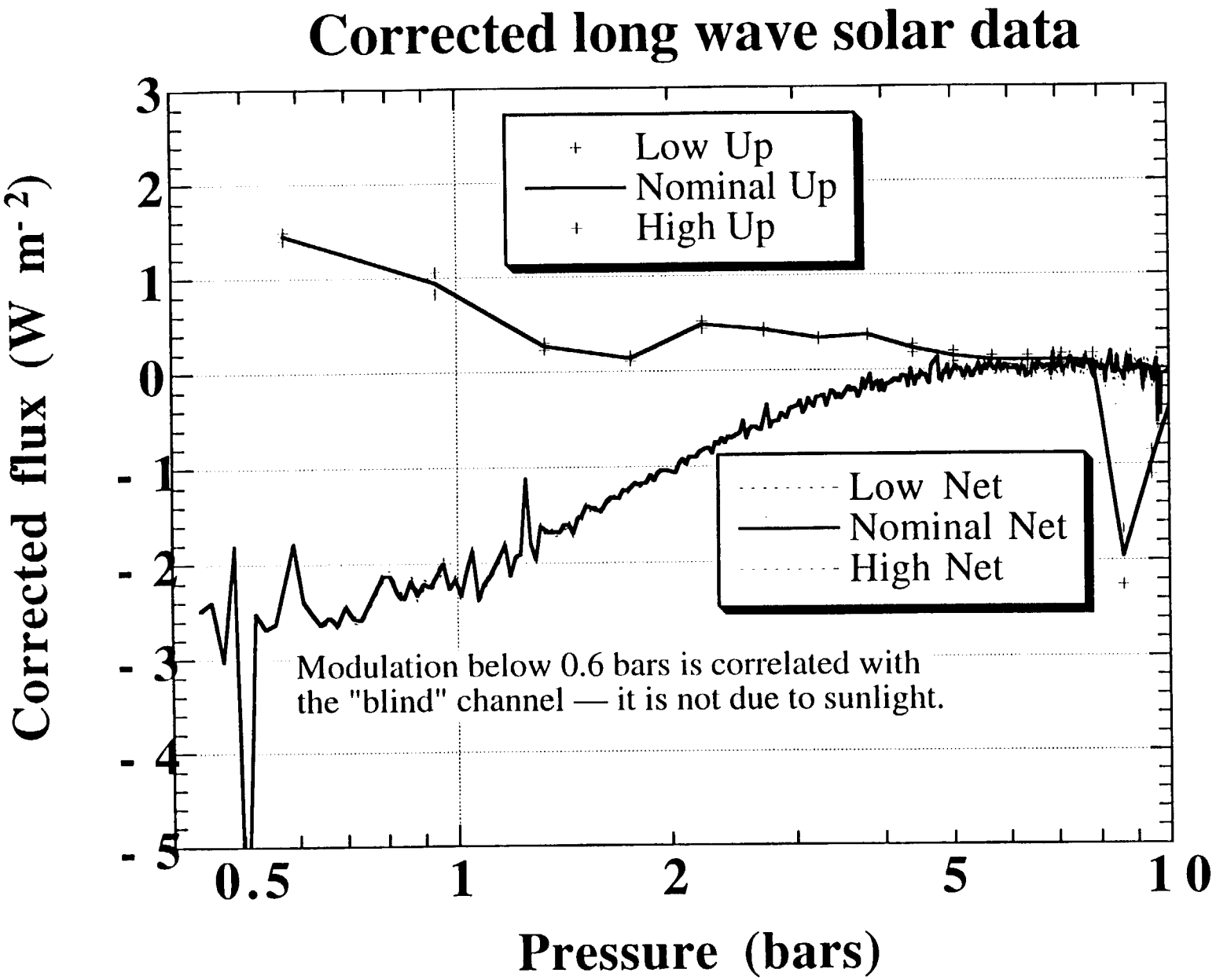
Corrected long wave solar data
Corrected flux (W m-2)
3
2
1
0
-1
-2
-3
-4
-5
0.5
1
2
5
10
Pressure (bars)
Low Up
Nominal Up
High Up
Low Net
Nominal Net
High Net
Modulation below 0.6 bars is correlated with
the "blind" channel — it is not due to sunlight.

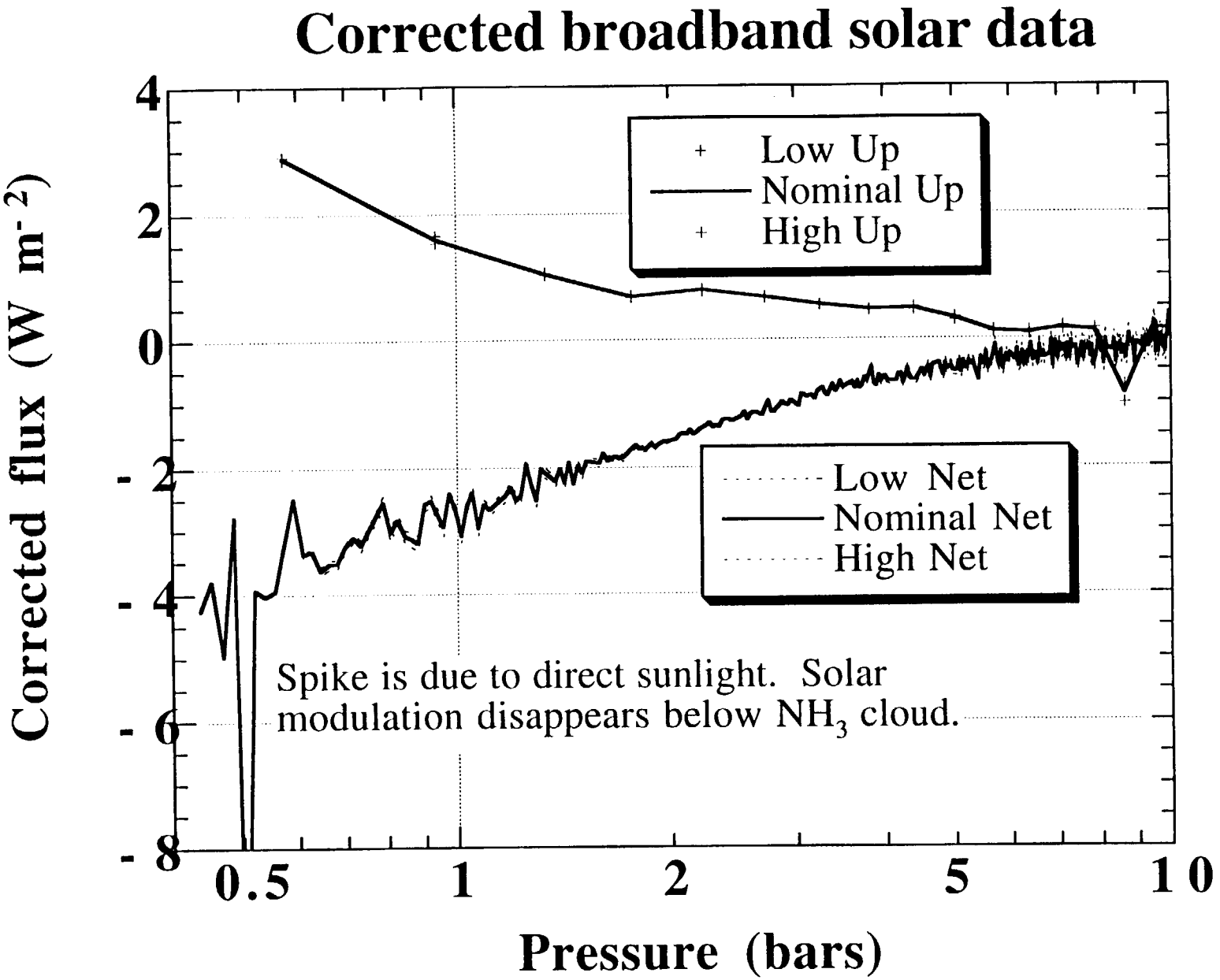
Corrected broadband solar data
Corrected flux (W m-2)
4
2
0
- 2
- 4
- 6
- 8
0.5
1
2
5
10
Pressure (bars)
Low Up
Nominal Up
High Up
Low Net
Nominal Net
High Net
Spike is due to direct sunlight. Solar modulation disappears below NH3 cloud.

Within the first several net flux measurements, there is a large amplitude modulation. This modulation has been identified as the contribution of direct sunlight (Sromovsky *et al.*, 1996, *Science* **272**, 851-854): as the NFR chops up and down, the probe is spinning at 30 to 40 RPM, and direct sunlight enters the field of view in some integrations, but not others. The interpretation of this contribution from direct sunlight is not very sensitive to the corrections for non-radiative effects, as those effects (as measured by the blind channel) were small at the beginning of the descent.

First, the solar modulation seen in the B-channel alone was studied. After taking into account the spatial field of view of the NFR, the chopping frequency, and the integration method, radiative transfer models were compared with the observed modulation for a variety of assumed spin rates and initial orientations. The best fit spin rate was 36.0 ± 0.15 RPM, consistent with LRD measurements of the probe spin rate (Lou Lanzerotti, personal communication); note that, because of various frequencies interacting, there are many other possible solutions in the 20 to 65 RPM range.

Below, 0.58 bars, this modulation was not observed. As the spin rate decays and the various frequencies beat with each other, the modulation can temporarily go away in the models, but in order to completely eliminate the modulation a cloud of optical depth near (or larger than) two is required. Thus, it has been argued that there is an ammonia ice cloud in the 0.5 to 0.6 bar region (Sromovsky *et al.* 1996).

Above 0.6 bars, the modulation in B is correlated with modulation in E, A, and C. The modulation in E is understood: given the relative amounts of sunlight in the two bandpasses, the modulation in E is expected to be about 50% (it can vary slowly with size of cloud particles) that in B, as is observed. The modulations in A and C are much larger than would be expected based only on the relative amounts of sunlight. The presence of small cloud particles (0.5 to 1 μm) above the site of the measurements (i.e., above 0.5 bars) can reduce the B and E modulation relative to the A and C modulation. However, this causes the modulation amplitudes to be consistently too small compared to the models. While Lemmon was in Wisconsin, possible mechanisms to boost the overall modulation amplitude were investigated. We were able to rule out small angle scattering—the modulation amplitude can be increased by scattering light into a solar aureole, because the Sun is at the edge of the NFR field of view, but the maximum increase is too small. We were also able to rule out pendulum type motion, including coning—the Sun is raised within the NFR field of view, giving a factor of four boost. Together with a 39 RPM spin rate this could reproduce all the observed modulation

amplitude, but only if the pendulum frequency were large compared to the 6-second integration or approximately the same as the rotation frequency—but it is about 5 seconds, which will not work. NFR observations alone cannot rule out a constant tilt of the probe, but such a tilt would have to fall within a narrow range of angles (about 19±2 degrees); and it has not been observed in the accelerometer data. It is possible that the presence of a thermal radiation source (such as a cloud) is the cause of the modulation in the thermal channels. In order to get similar phasing of the modulation between the solar and thermal channels, the cloud would have to fall within a narrow size range (too big and it is seen often—there is little or no modulation; too small and there is not enough signal within the NFR field of view) and would have to be in just the right position. Thus, we do not yet have a good explanation of the modulation observed in the thermal channels.

Radiative transfer models

The capability to invert the net and up flux measurements in order to get a profile of scattering and absorption in the atmosphere was developed at the UA. This inversion was performed on the best calibration of the data and reported on at the 1996 DPS meeting (Lemmon *et al.* 1996), but the up flux measurements are not yet believed.

Inversion process

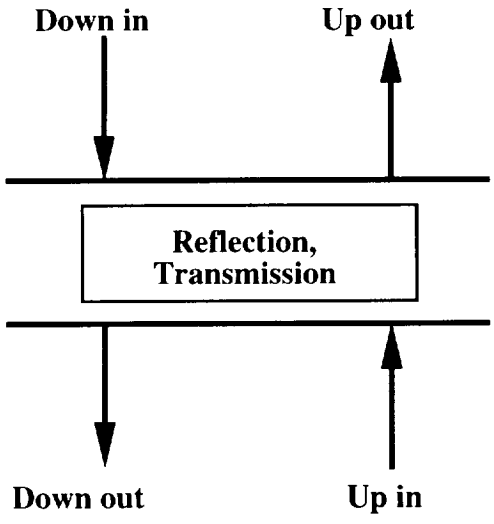

A layer is defined between two measurements of the up flux. The up and net fluxes are combined into down fluxes. Given up and down fluxes at the top and bottom of the layer, the layer's reflection and transmission properties are uniquely defined by the relations:

$$D_{out} = \mathbf{T} \bullet D_{in} + \mathbf{R} \bullet U_{in} \quad (1)$$

$$U_{out} = \mathbf{T} \bullet U_{in} + \mathbf{R} \bullet D_{in} \quad (2)$$

Figure 2: Layer definition

where T and R are the effective layer transmission and reflection for the bandpass. These describe the effects of layer opacity, but also respond to effects such as sunset and

the NFR spatial response, which must be included in the model. Parts of the layer opacity are the (relatively) well-known methane absorption and Rayleigh scattering, which are included in the model, and parts are unknown. The latter is the target of the inversion. The up flux has been corrected for perturbations and points have been selected to avoid pathological conditions such as negative up fluxes or large increases of up flux with depth. The down flux is (*up* - *net*), where the net flux has been appropriately corrected and sampled in the region of the up flux measurement.

A standard Jupiter model was created. This model has methane, hydrogen, and helium, and has a haze in the troposphere A cloud with optical depth 0.5 has been added between 0.5 and 0.58 bars due to the observation of a disappearance of the solar modulation. At this stage, the exact nature of scattering above 0.58 bars (the first UF measurement) is unimportant—the T and R properties of the layer respond primarily to opacity within the layer. Opacity outside of a particular layer has a second order effect within the layer by changing the spectral distribution of light entering the layer.

When this model is run, the quantity ($1-T-R$), which is a good measure of absorption and responds only weakly to scattering, has non-zero values due to the methane absorption and sunset. The quantity R (or $R/(R+T)$), which is a good measure of scattering (the latter responds weakly to absorption), has non zero values due to Rayleigh scattering. The algorithm is to iterate a perturbation method as follows. The sensitivity of the layer properties (generically used to indicate R and T) to the addition of scattering and absorption opacity is separately tested. A next generation model is created where opacity is added to each layer in an attempt to fit the measurements. This is continued until a satisfactory fit is achieved. Note that the successful completion of this process does not guarantee a fit to the data—the layer properties, as defined by changes in flux within a layer, are fit. Given the negligible up flux at the bottom of the measurements (near sunset), if the down flux at 0.58 bars in the model matches that which was observed, the fit will be exact. Otherwise, the up and net fluxes predicted by the model will differ from that observed by a factor of $D_{top\text{-}of\text{-}atmosphere,model} / D_{top\text{-}of\text{-}atmosphere,observed}$.

The above algorithm is first applied to the E channel data. After successful inversion, the opacities longward of 0.65 μm are held fixed while the opacities for shorter wavelengths are allowed to vary. If the B and E channel data are inconsistent (*e.g.*, B requires little opacity in a given layer, and the opacity in E is so large that even zero opacity short of 0.65 μm provides too large an effect), the inversion will fail here.

Inversion results

The model (Fig. 3) can be made to fit the long wave (E) channel data arbitrarily well by adjusting the layer scattering and absorption properties. After these opacities are determined for wavelengths greater than 0.65 μm (to which E is sensitive), the broad band (B) channel data cannot be fit arbitrarily well. In all cases, if the E channel data are fit, there is too much scattering opacity for the B channel to be fit, even when the scattering opacity is set to zero for wavelengths less than 0.65 μm. The model can be compared to the LRD radiance data (Lanzerotti et al., Science 272, 858-60, 1996), as in Fig 4. The LRD spectral dependence is similar to the NFR E channel; thus the profile cannot be fit while simultaneously having the up and net fluxes fit the corrected E channel data, because the NFR sees the brightness falling off higher in the atmosphere.

The aerosol structure retrieved has a blue-scattering cloud above 1 bar (in addition to the presumed cloud at 0.55—0.6 bars). Also, a red-scattering cloud below 3 bars is required, although we do not have a physical analog for this feature. In addition, a red absorber is required in the 1 to 5 bar region in order to reduce the E net flux (there is only weak absorption at shorter wavelengths). The absorber in question cannot be CH4. Methane absorption is already accounted for before introducing aerosol opacity. Further, uncertainty in methane absorption coefficients is unable to account for the red absorber.

The solar heating rate can be calculated for the model, and averaged over a Jovian day (Fig. 5). It is somewhat model independent, as the solar net flux profile must look much like the B channel net flux profile. The solar heating rate is sensitive to uncertainties in the scheme for removing the non-radiative terms, as it is determined from the gradient of the solar net flux profile.

Publications

Sromovsky, Best, Collard, Fry, Revercomb, Freedman, Orton, Hayden, Tomasko, and Lemmon 1996. Solar and thermal radiation in Jupiter's atmosphere: Initial results of the Galileo probe Net Flux Radiometer. *Science* **272**, 851-854.

Conference Presentations

Sromovsky, L.A., A.D. Collard, P.M. Fry, H.E. Revercomb, F.A. Best, G.S. Orton, M.G. Tomasko, M.T. Lemmon, R.F. Freedman, and J. Hayden. Preliminary results of the Galileo Net Flux Radiometer experiment. **LPSC**

Sromovsky, Collard, Fry, Revercomb, Best, Orton, Tomasko, Lemmon, Freedman, and Hayden. Early results of the Galileo Net Flux Radiometer Experiment. **AGU**

Model fit to corrected long wave solar data

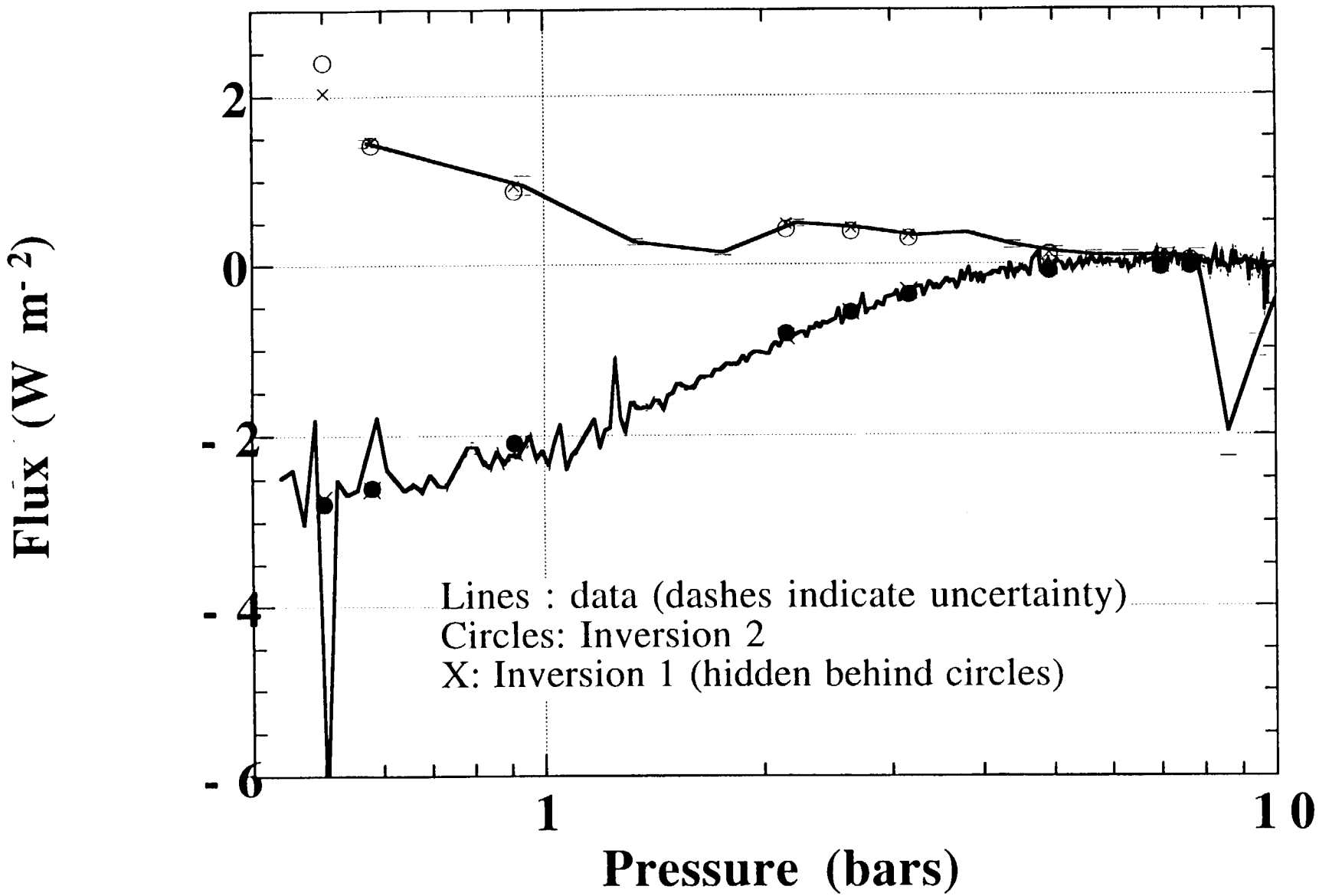

Model fit to corrected broad band solar data

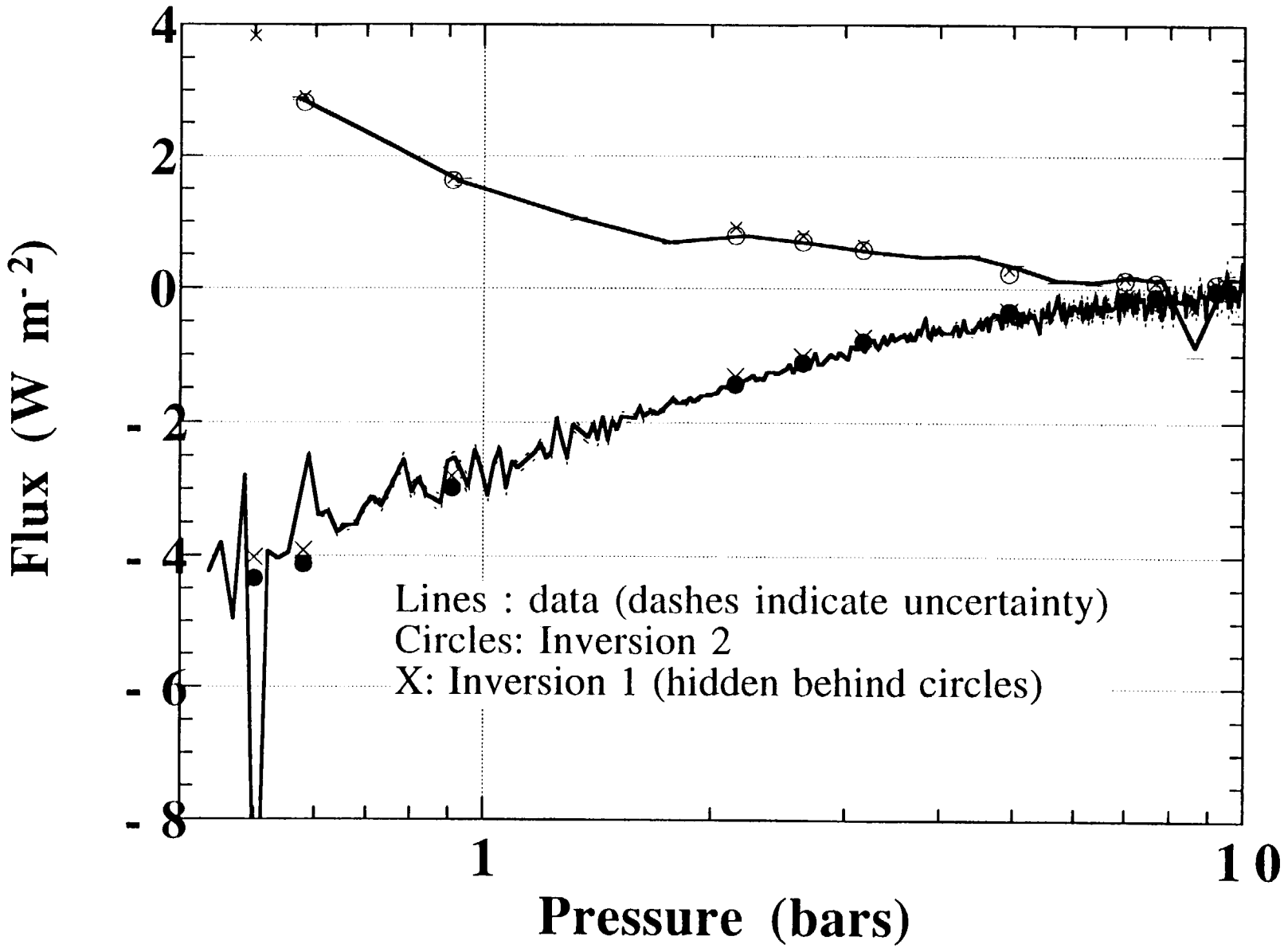

Comparison to LRD radiance data

Data courtesy of Lanzerotti et al. (Science 272, 858-60, 1996)

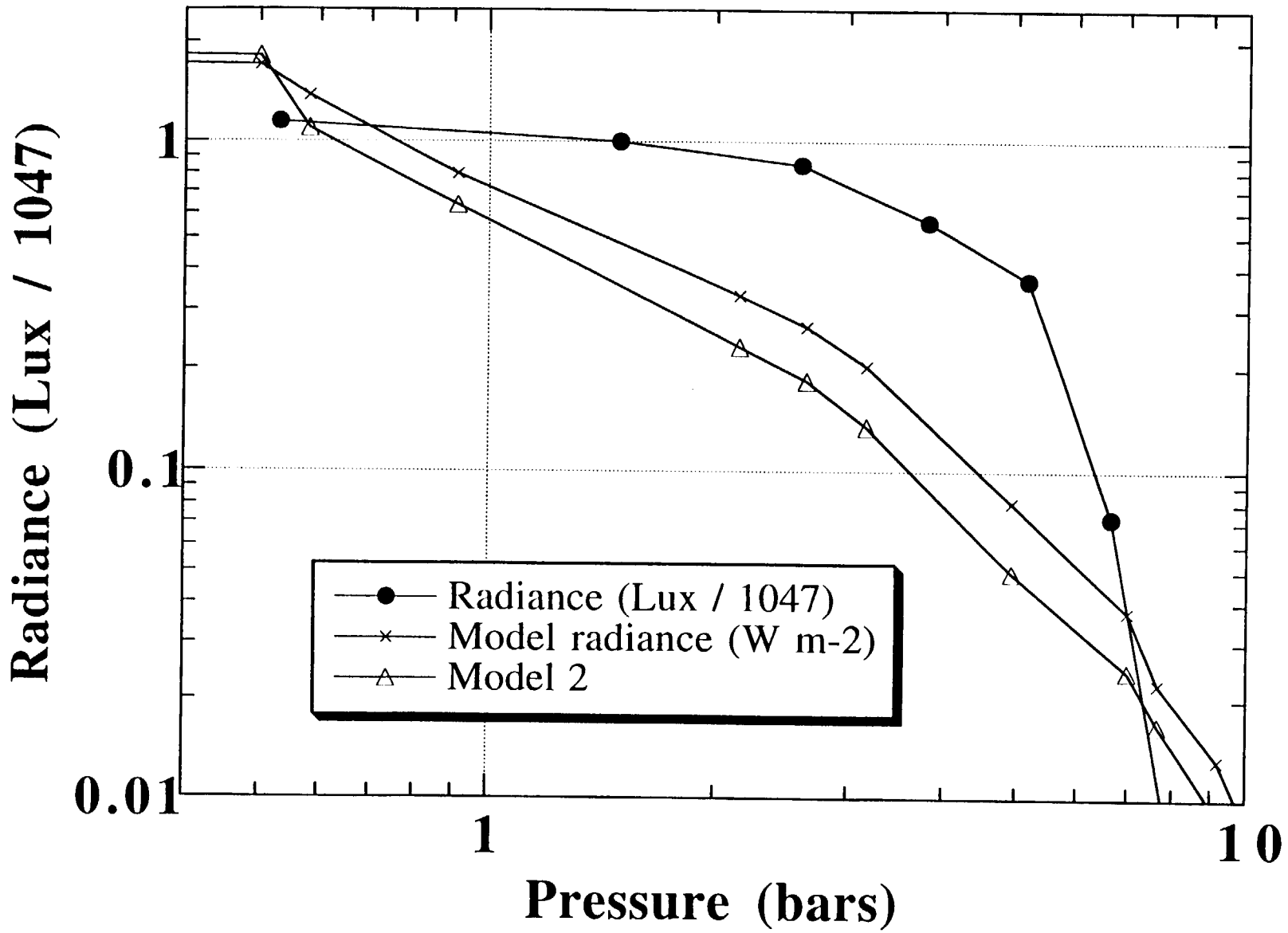

Solar heating at Galileo Hot Spot, 7 December 1995

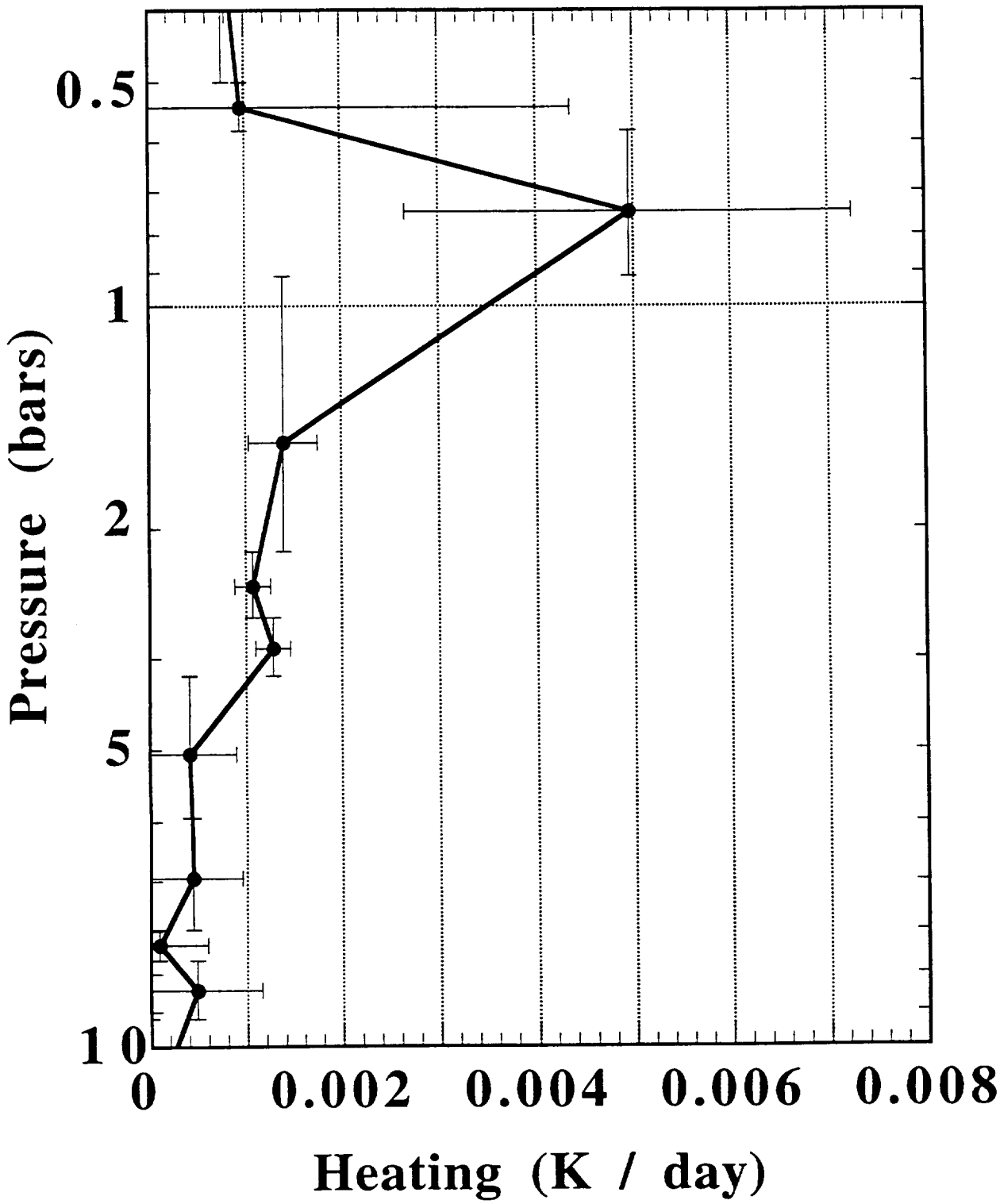

Lemmon, Tomasko, Sromovsky, and Collard. Inversion of Galileo Net Flux Radiometer results for Cloud Properties. **DPS**

Collard, Sromovsky, Fry, Orton, Lemmon, and Tomasko. Thermal Radiative Fluxes in Jupiter's Atmosphere: Implications of the Galileo Probe Net Flux Radiometer Results. **DPS**